Electronic Supplementary Information

Particle/Cell Separation Using Sheath-Free Deterministic Lateral Displacement Arrays with Inertially Focused Single Straight Input

*Naotomo Tottori, and Takasi Nisisako**

Institute of Innovative Research, Tokyo Institute of Technology, Yokohama, Japan

Supplemental Text

Principle of inertial focusing in a straight microchannel

The particles flowing in a straight microchannel migrate to equilibrium positions determined by the balance between the inertial lift forces. One of these forces is induced by the curvature of the velocity profile and is referred to as the shear-induced lift force (F_s), while another is induced by the interaction between the particles and the channel walls and is referred to as the wall-induced lift force (F_w) (Ref. 31). In a straight microchannel with a radially asymmetric (e.g., rectangular) cross section, the migration of the particles consists of two stages (Ref. 35). The particles first migrate toward the long channel faces and reach their first equilibrium position when F_s and F_w balance each other. Thereafter, they migrate toward the middle of the channel between the two wider sidewalls under the action of a rotation-induced lift force (F_Ω).

Supplemental Figures and Tables
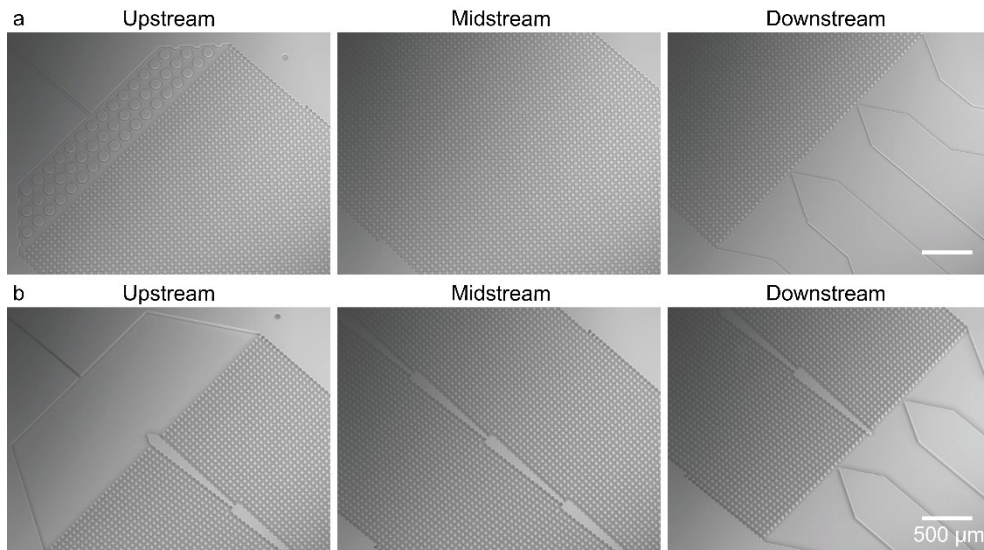
Fig. S1 Scanning electron microscope images of the DLD array of the (a) CF-DLD and (b) SF-DLD.
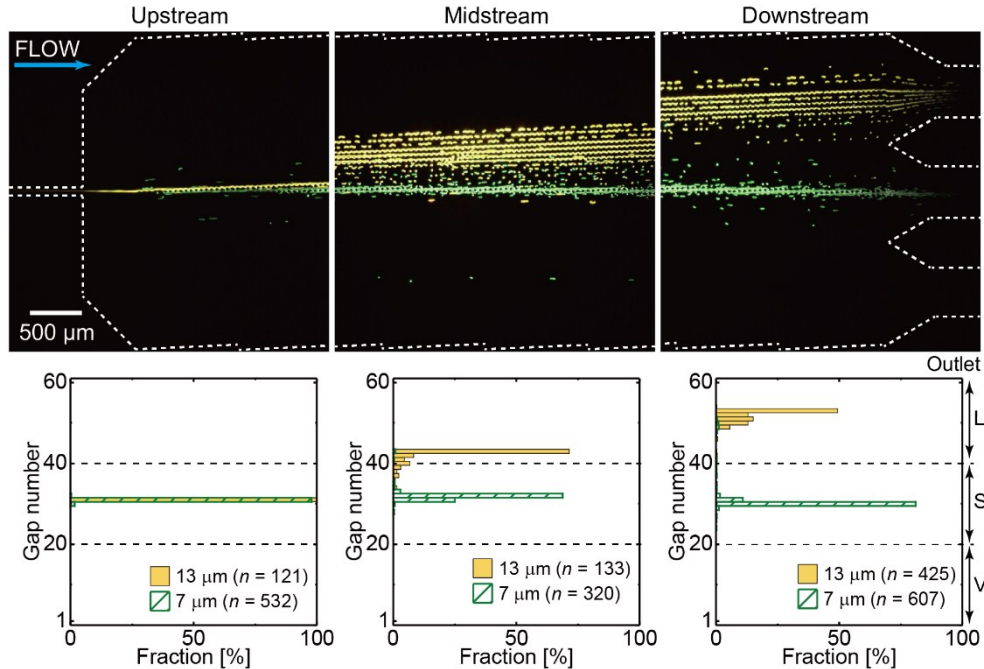
Fig. S2 Trajectories and spatial distributions of the 13 μm (yellow) and 7 μm (green) beads flowing upstream, midstream, and downstream within the DLD region of the CF-DLD at $Q = 5.0$ mL h^{-1}. The white dashed lines indicate the sidewalls. The number of particles over 10 s was counted in sections 1, 12, and 23 of the DLD array.
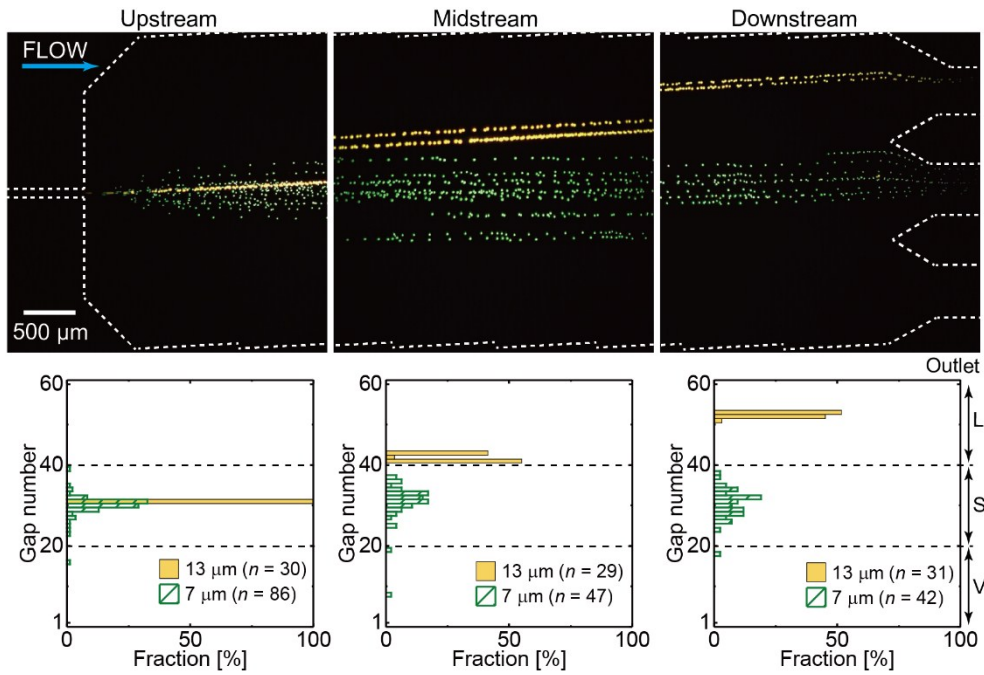
Fig. S3 Trajectories and spatial distributions of the 13 μm (yellow) and 7 μm (green) beads flowing within the DLD region of the CF-DLD at $Q = 1.0$ mL h^{-1}. The number of particles over 10 s was counted in sections 1, 12, and 23 of the DLD array.
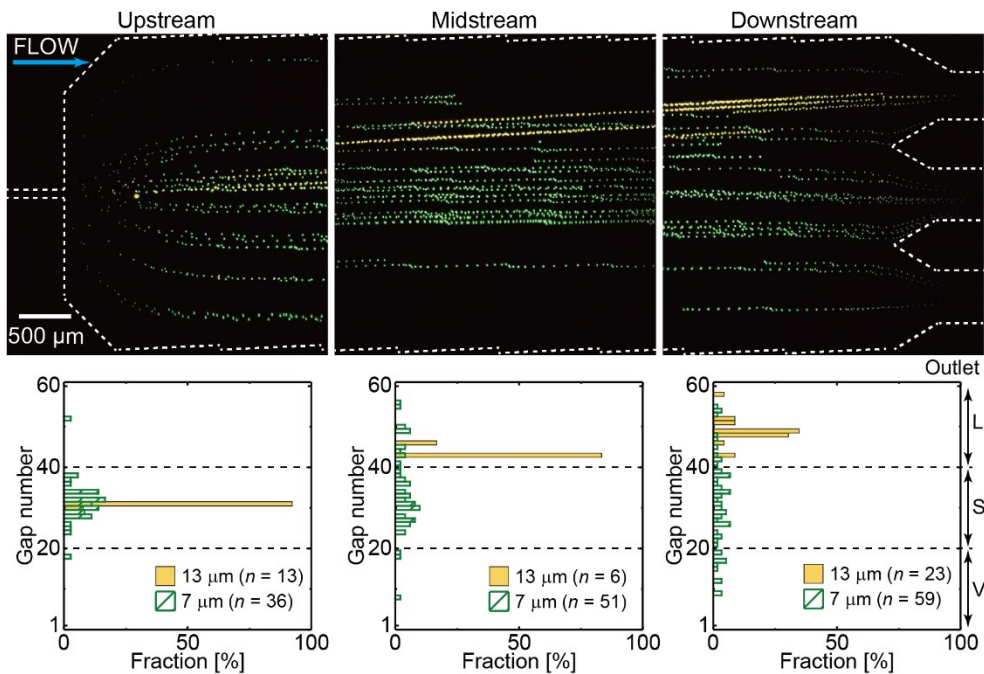
Fig. S4 Trajectories and spatial distributions of the 13 μm (yellow) and 7 μm (green) beads flowing within the DLD region of the CF-DLD at $Q = 0.5$ mL h^{-1}. The number of particles over 10 s was counted in sections 1, 12, and 23 of the DLD array.
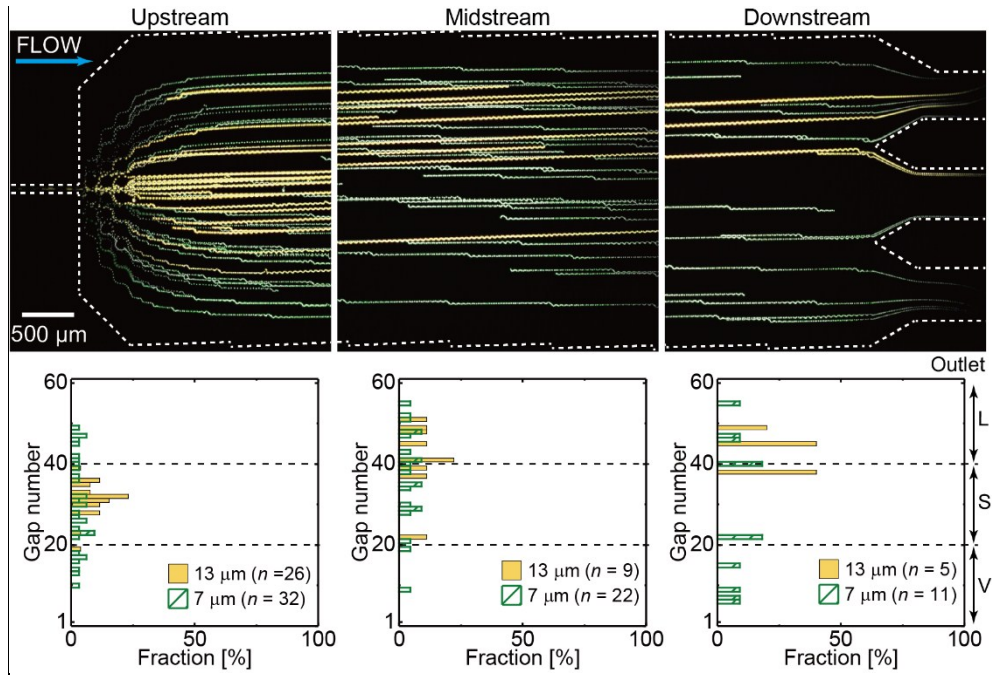
Fig. S5 Trajectories and spatial distributions of the 13 μm (yellow) and 7 μm (green) beads flowing within the DLD region of the CF-DLD at $Q = 0.1$ mL h^{-1}. The number of particles over 40 s was counted in sections 1, 12, and 23 of the DLD array.
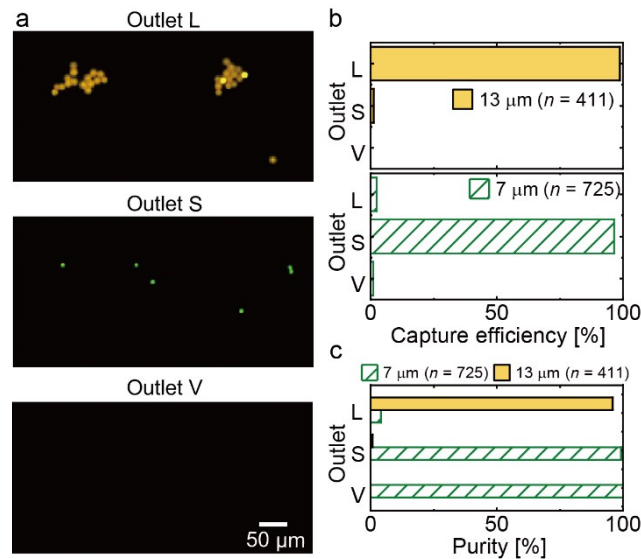
Fig. S6 Separation of particles of different sizes using the CF-DLD ($Q = 5.0$ mL h^{-1}). (a) Fluorescence microscopy images of the particles collected at the three outlets. (b) Capture efficiencies for the 13 and 7 μm beads. (c) Purities of the 13 and 7 μm beads at each outlet.
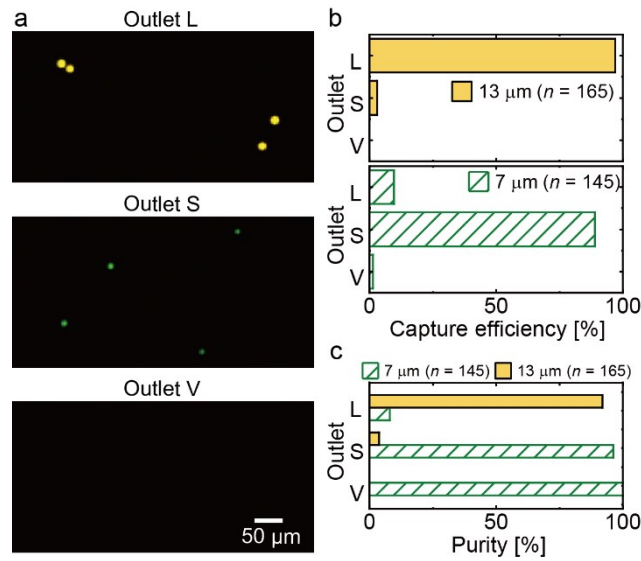
Fig. S7 Separation of particles of different sizes using the CF-DLD ($Q = 1.0$ mL h^{-1}). (a) Fluorescence microscopy images of the particles collected at the three outlets. (b) Capture efficiencies for the 13 and 7 µm beads. (c) Purities of the 13 and 7 µm beads at each outlet.
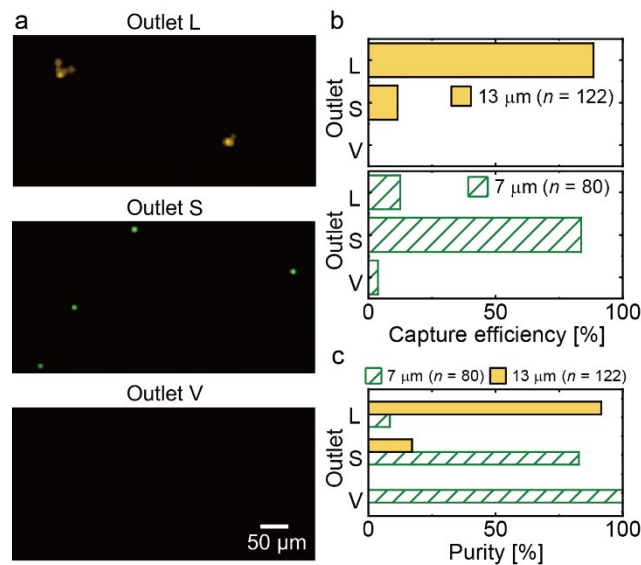
Fig. S8 Separation of particles of different sizes using the CF-DLD ($Q = 0.5$ mL h^{-1}). (a) Fluorescence microscopy images of the particles collected at the three outlets. (b) Capture efficiencies for the 13 and 7 µm beads. (c) Purities of the 13 and 7 µm beads at each outlet.
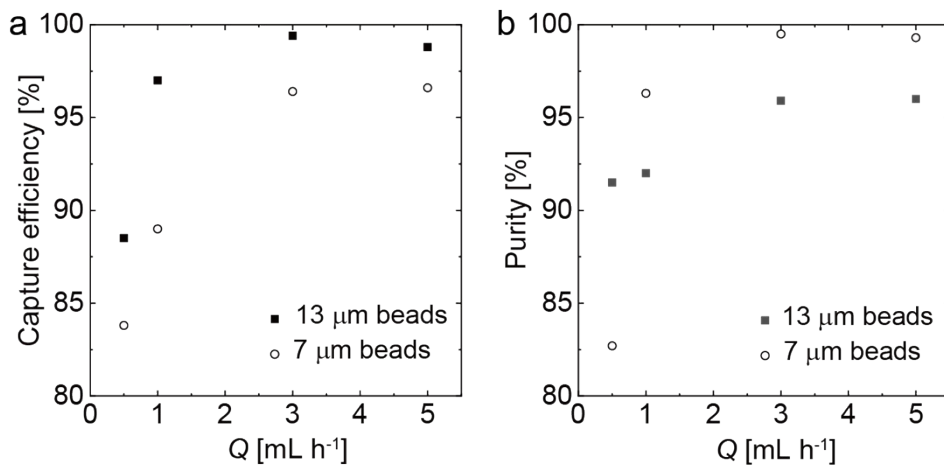
Fig. S9 Separation performance of the CF-DLD with respect to the flow rate. (a) Capture efficiencies for the 13 and 7 μm beads collected at outlets L and S. (b) Purities of the 13 and 7 μm beads collected at outlets L and S.
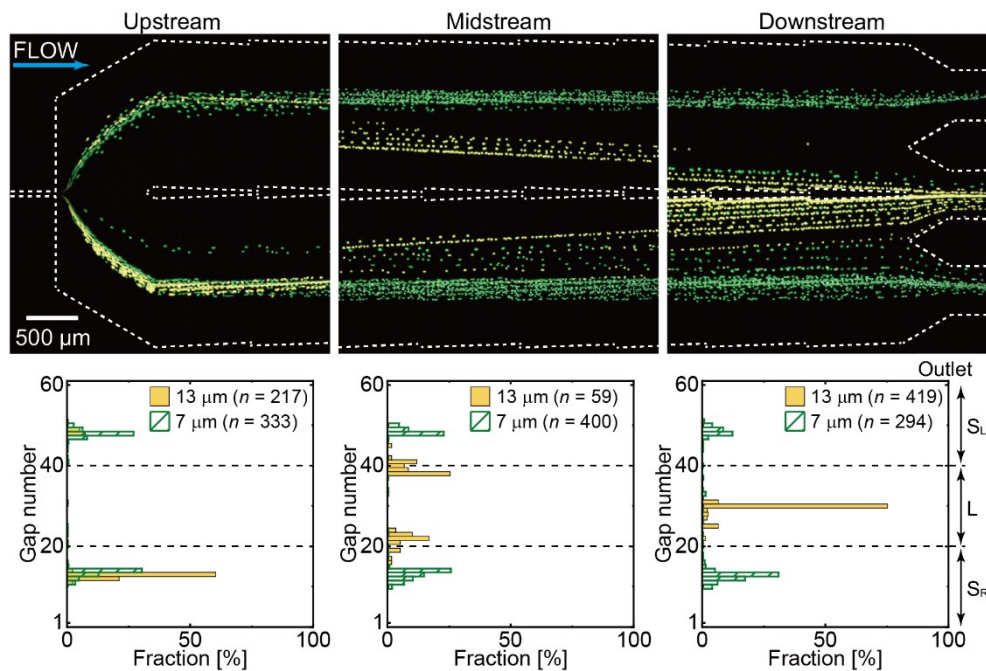
Fig. S10 Trajectories and spatial distributions of the 13 μm (yellow) and 7 μm (green) beads flowing upstream, midstream, and downstream within the DLD region of the SF-DLD with 2 mm inertial focusing channel at $Q = 3.0$ mL h^{-1}. The number of particles over 10 s was counted in sections 1, 12, and 23 of the DLD array.
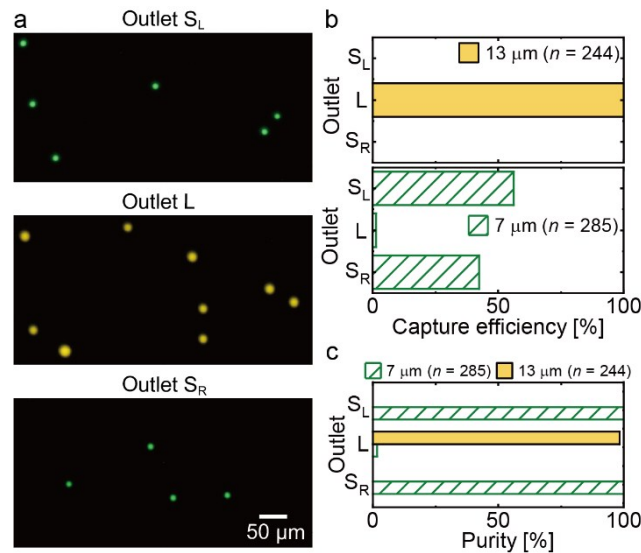
Fig. S11 Separation of particles of different sizes using the SF-DLD with 2mm inertial focusing channel ($Q = 3.0$ mL h^{-1}). (a) Fluorescence microscopy images of the particles collected at the three outlets. (b) Capture efficiencies for the 13 and 7 μm beads. (c) Purities of the 13 and 7 μm beads at each outlet.
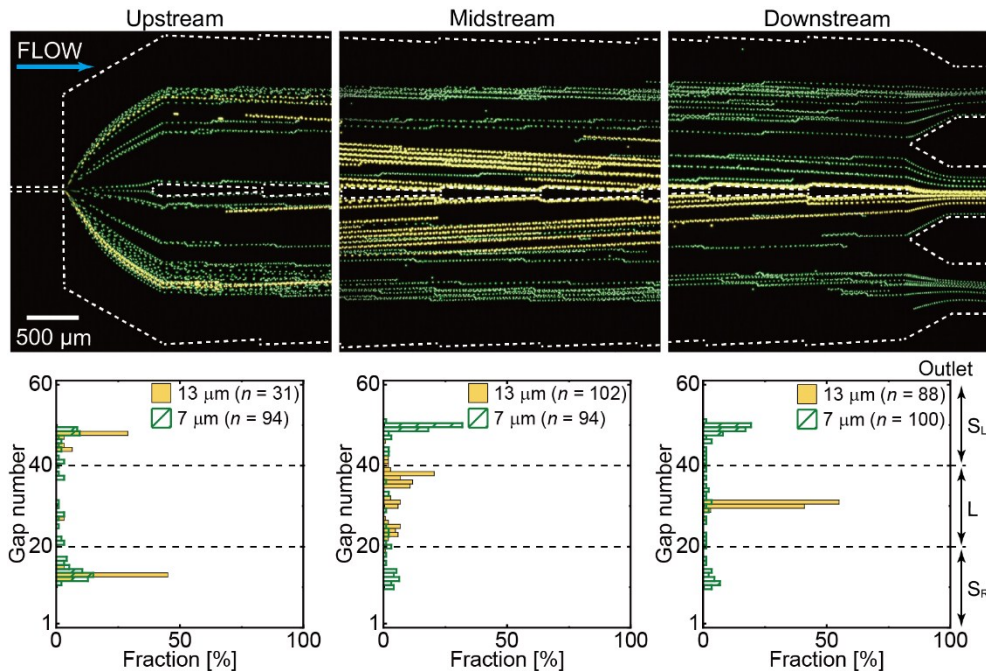
Fig. S12 Trajectories and spatial distributions of the 13 μm (yellow) and 7 μm (green) beads flowing upstream, midstream, and downstream within the DLD region of the SF-DLD with 2 mm inertial focusing channel at $Q = 0.5$ mL h^{-1}. The number of particles over 30 s was counted in sections 1, 12, and 23 of the DLD array.
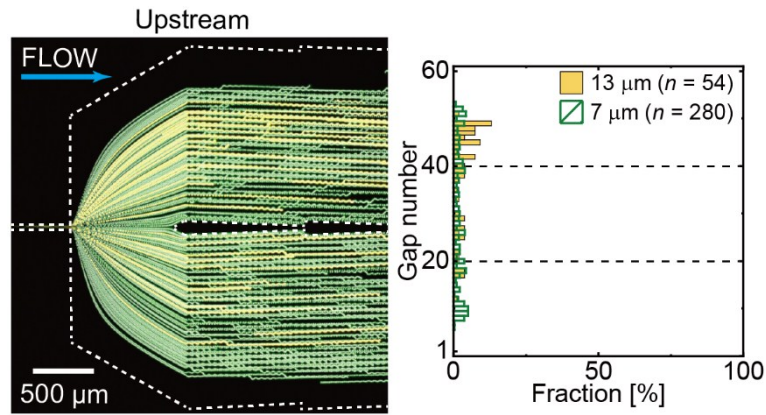
Fig. S13 Trajectories and spatial distributions of the 13 μm (yellow) and 7 μm (green) beads flowing upstream within the DLD region of the SF-DLD with 2 mm inertial focusing channel at $Q = 0.1$ mL h^{-1}. The number of particles over 130 s was counted in sections 1 of the DLD array.
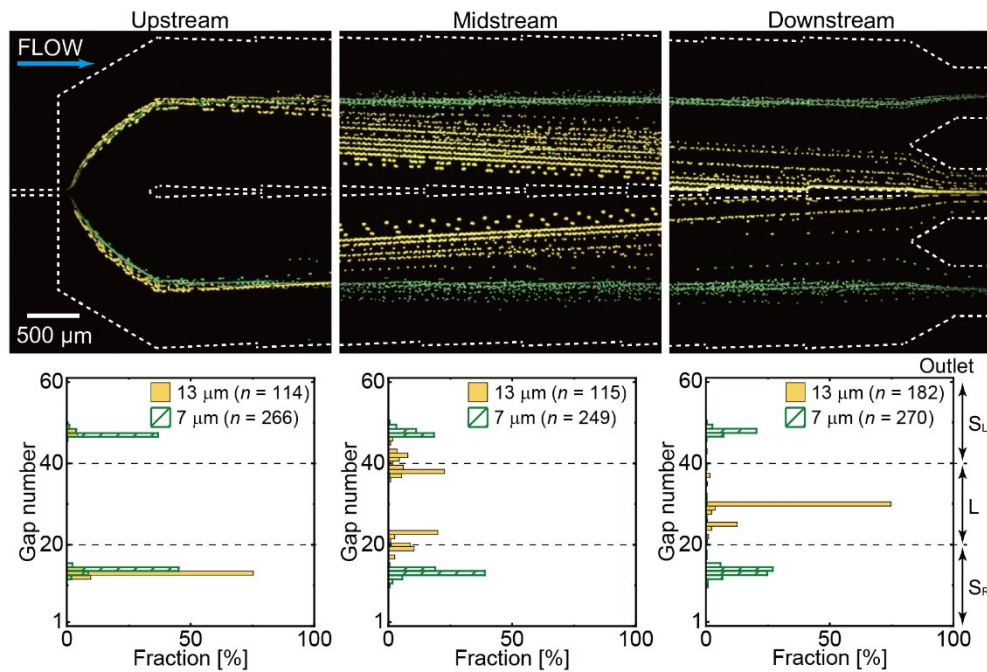
Fig. S14 Trajectories and spatial distributions of the 13 μm (yellow) and 7 μm (green) beads flowing upstream, midstream, and downstream within the DLD region of the SF-DLD with 5 mm inertial focusing channel at $Q = 3.0$ mL h^{-1}. The number of particles over 10 s was counted in sections 1, 12, and 23 of the DLD array.
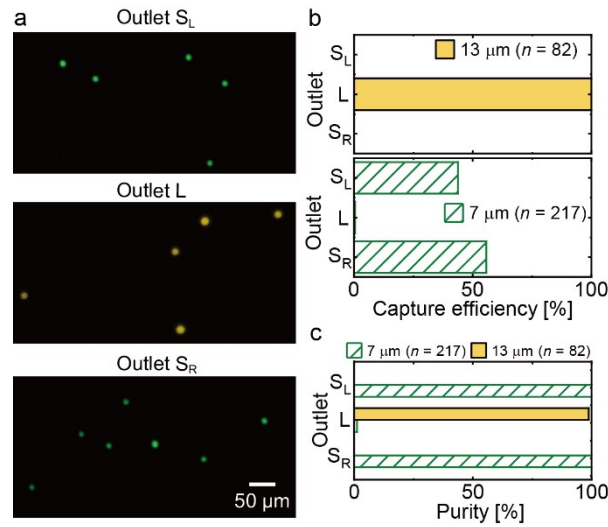
Fig. S15 Separation of particles of different sizes using the SF-DLD with 5 mm inertial focusing channel ($Q = 3.0$ mL h^{-1}). (a) Fluorescence microscopy images of the particles collected at the three outlets. (b) Capture efficiencies for the 13 and 7 μm beads. (c) Purities of the 13 and 7 μm beads at each outlet.
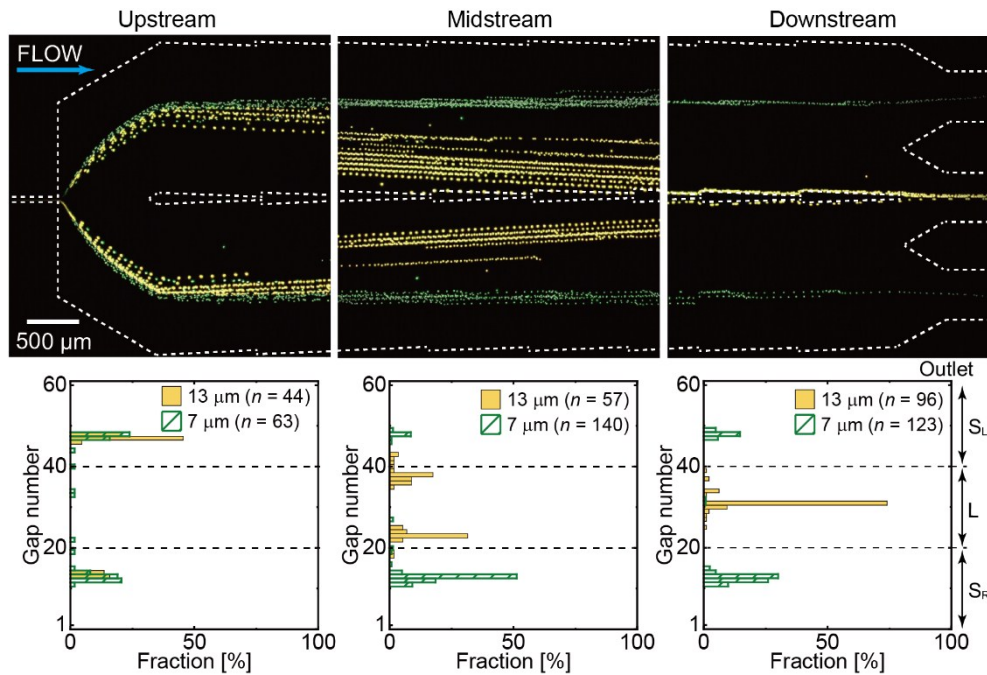
Fig. S16 Trajectories and spatial distributions of the 13 μm (yellow) and 7 μm (green) beads flowing upstream, midstream, and downstream within the DLD region of the SF-DLD with 5 mm inertial focusing channel at $Q = 1.0$ mL h^{-1}. The number of particles over 30 s was counted in sections 1, 12, and 23 of the DLD array.
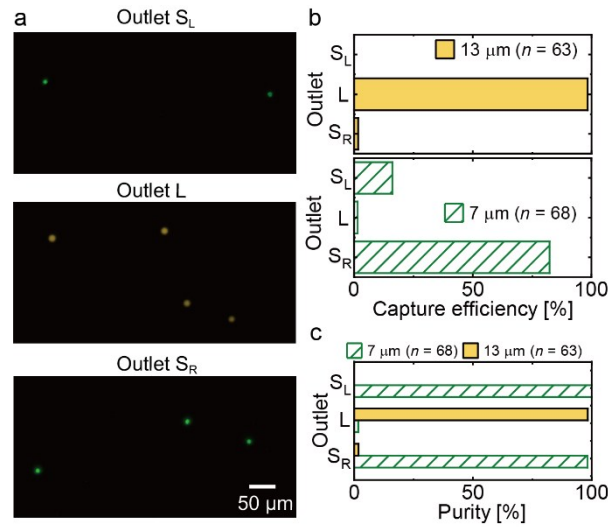
Fig. S17 Separation of particles of different sizes using the SF-DLD with 5 mm inertial focusing channel ($Q = 1.0$ mL h^{-1}). (a) Fluorescence microscopy images of the particles collected at the three outlets. (b) Capture efficiencies for the 13 and 7 μm beads. (c) Purities of the 13 and 7 μm beads at each outlet.
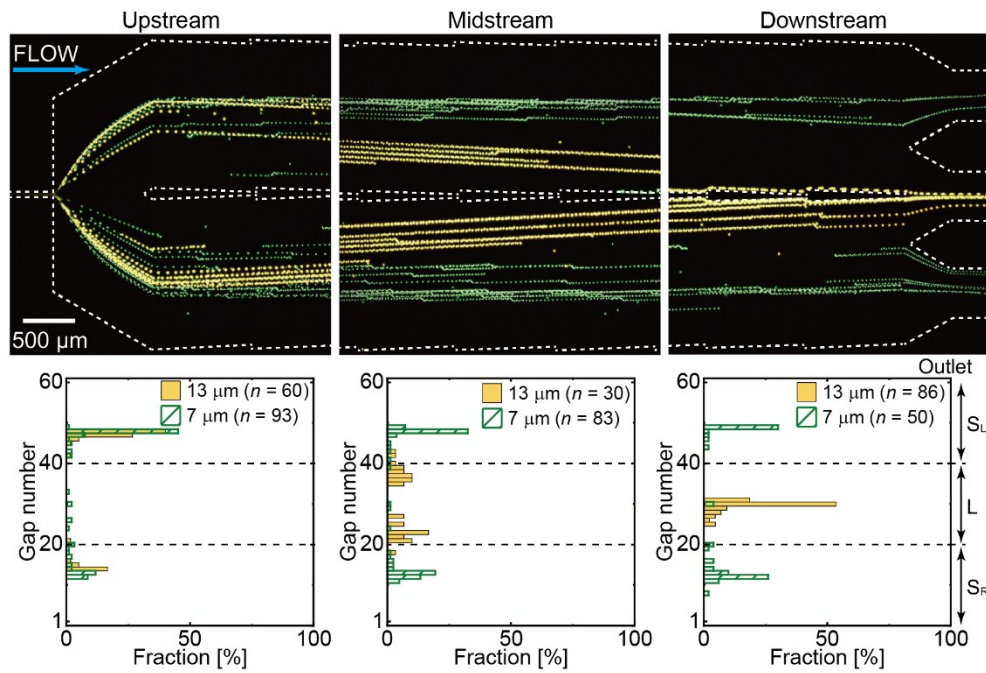
Fig. S18 Trajectories and spatial distributions of the 13 μm (yellow) and 7 μm (green) beads flowing upstream, midstream, and downstream within the DLD region of the SF-DLD with 5 mm inertial focusing channel at $Q = 0.5$ mL h^{-1}. The number of particles over 30 s was counted in sections 1, 12, and 23 of the DLD array.
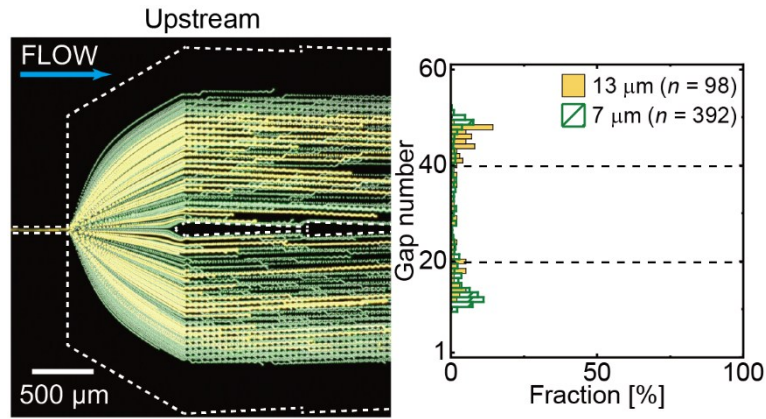
Fig. S19 Trajectories and spatial distributions of the 13 μm (yellow) and 7 μm (green) beads flowing upstream within the DLD region of the SF-DLD with 5 mm inertial focusing channel at $Q = 0.1$ mL h^{-1}. The number of particles over 130 s was counted in sections 1 of the DLD array.
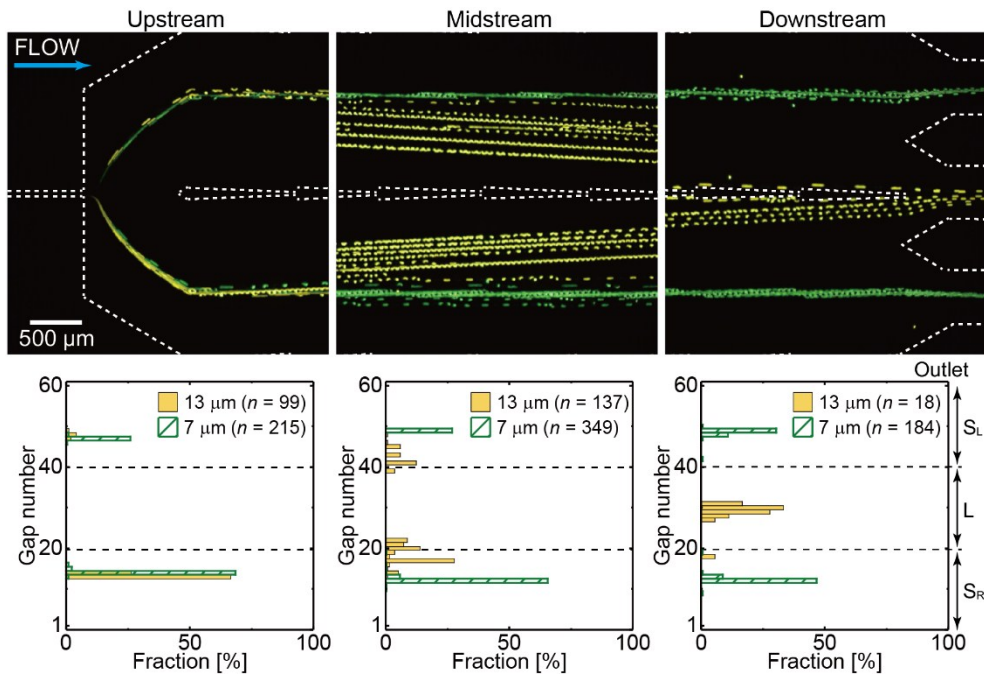
Fig. S20 Trajectories and spatial distributions of the 13 μm (yellow) and 7 μm (green) beads flowing upstream, midstream, and downstream within the DLD region of the SF-DLD with 20 mm inertial focusing channel at $Q = 3.0$ mL h^{-1}. The number of particles over 10 s was counted in sections 1, 12, and 23 of the DLD array.
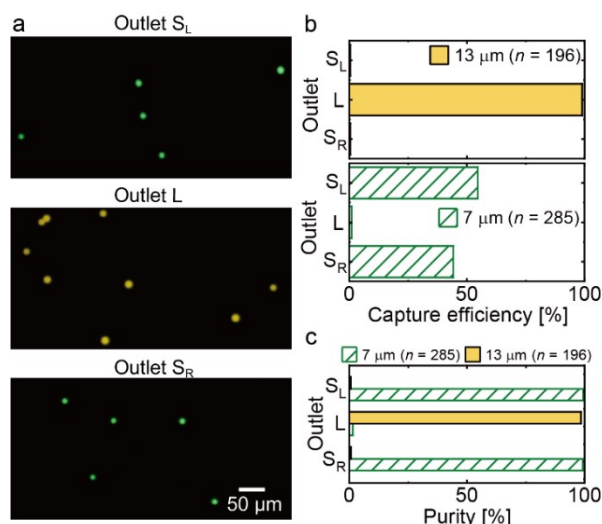
Fig. S21 Separation of particles of different sizes using the SF-DLD with 20 mm inertial focusing channel (Q = 3.0 mL h^{-1}). (a) Fluorescence microscopy images of the particles collected at the three outlets. (b) Capture efficiencies for the 13 and 7 μm beads. (c) Purities of the 13 and 7 μm beads at each outlet.
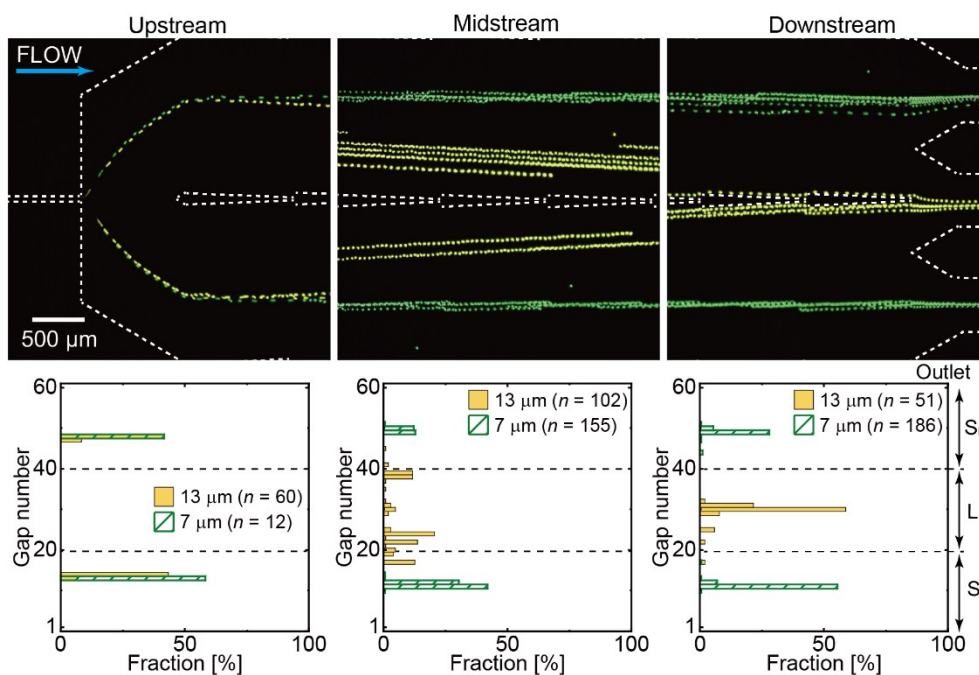
Fig. S22 Trajectories and spatial distributions of the 13 μm (yellow) and 7 μm (green) beads flowing upstream, midstream, and downstream within the DLD region of the SF-DLD with 20 mm inertial focusing channel at Q = 1.0 mL h^{-1}. The number of particles over 30 s was counted in sections 1, 12, and 23 of the DLD array.
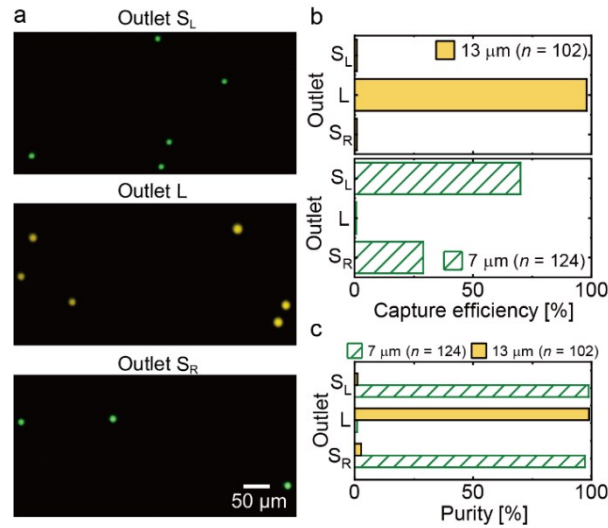
Fig. S23 Separation of particles of different sizes using the SF-DLD with 20 mm inertial focusing channel (Q = 1.0 mL h^{-1}). (a) Fluorescence microscopy images of the particles collected at the three outlets. (b) Capture efficiencies for the 13 and 7 μm beads. (c) Purities of the 13 and 7 μm beads at each outlet.
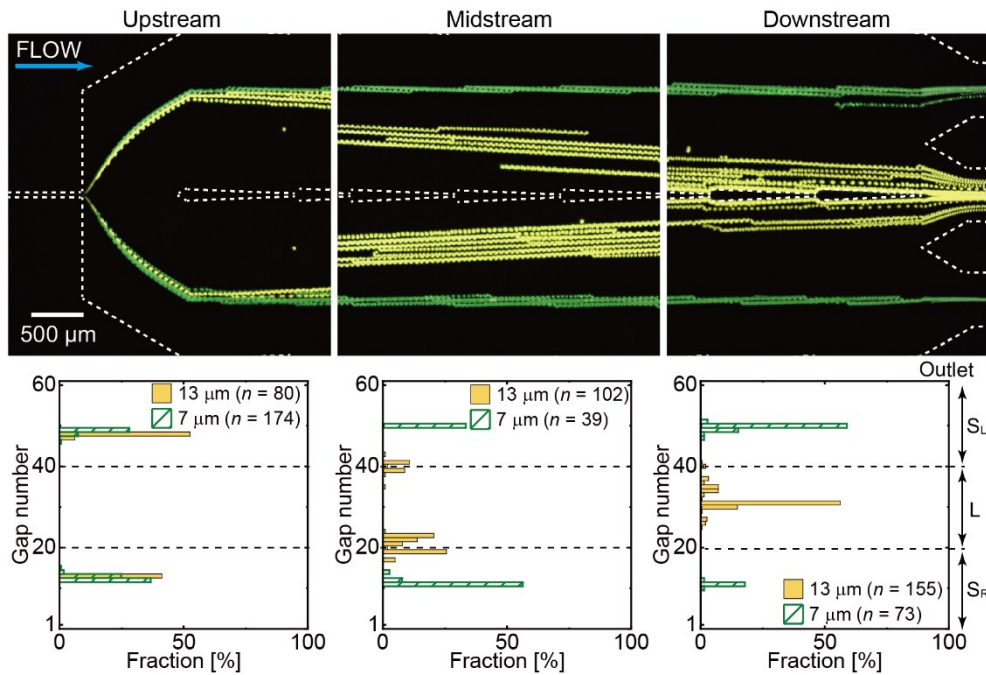
Fig. S24 Trajectories and spatial distributions of the 13 μm (yellow) and 7 μm (green) beads flowing upstream, midstream, and downstream within the DLD region of the SF-DLD with 20 mm inertial focusing channel at Q = 0.5 mL h^{-1}. The number of particles over 30 s was counted in sections 1, 12, and 23 of the DLD array.
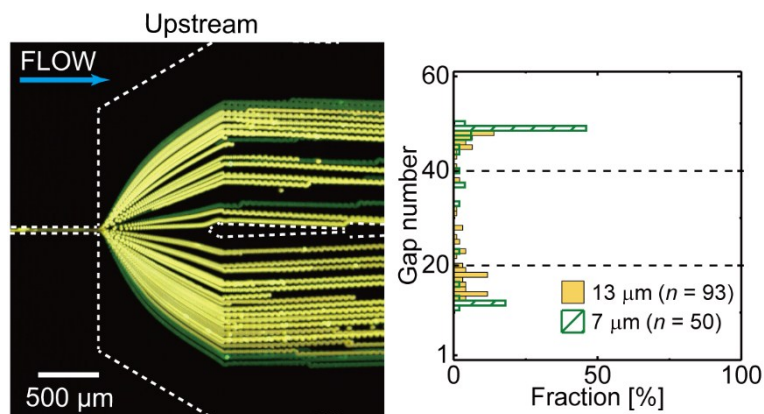
Fig. S25 Trajectories and spatial distributions of the 13 μm (yellow) and 7 μm (green) beads flowing upstream within the DLD region of the SF-DLD with 20 mm input channel at Q = 0.1 mL h^{-1}. The number of particles over 130 s was counted in section 1 of the DLD array.
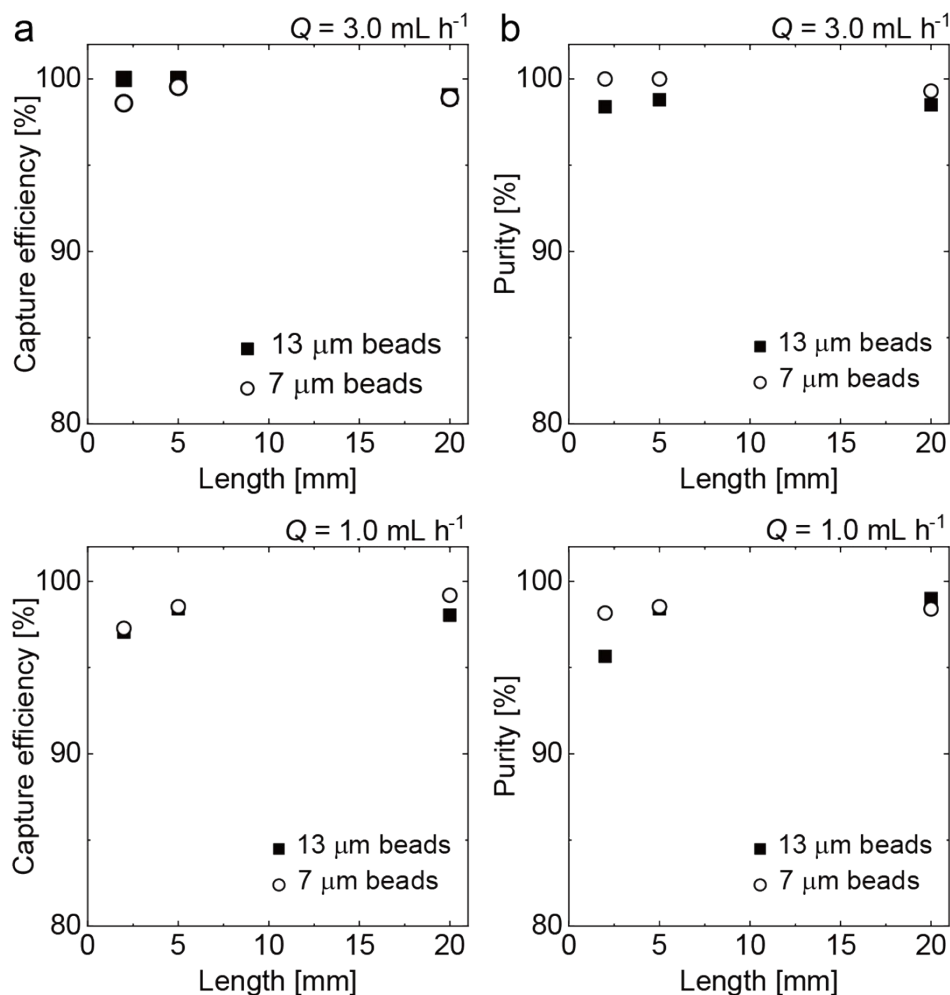
Fig. S26 Separation performance of the SF-DLD with respect to the channel length for inertial focusing at Q = 3.0 mL h^{-1} and 1.0 mL h^{-1} (a) Capture efficiencies for the 13 and 7 μm beads collected at outlets L and S. (b) Purities of the 13 and 7 μm beads collected at outlets L and S.
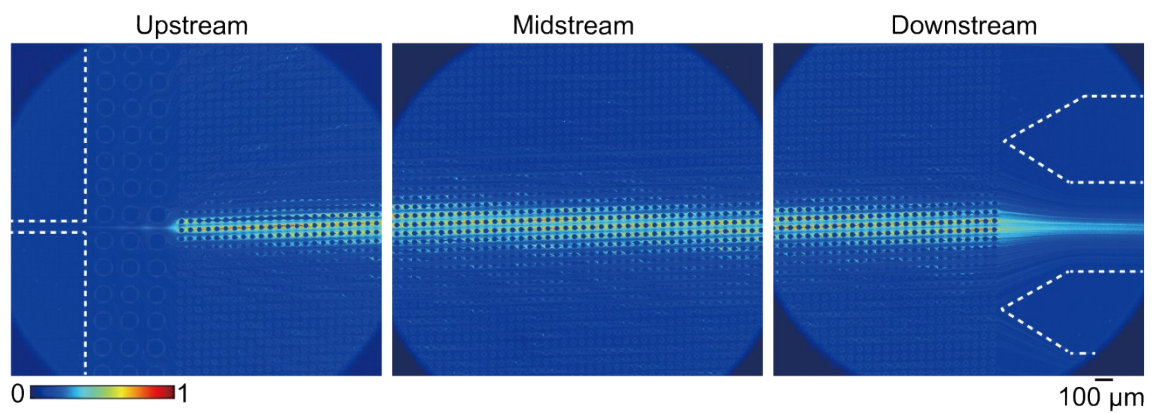
Fig. S27 Standard deviation (STD) plots of the trajectories of the cells flowing upstream, midstream, and downstream within the DLD region of the CF-DLD for $Q = 5.0$ mL h^{-1}.

Table S1 Comparison of the predicted focusing regimes by Equation 1 and experimental particle focusing regimes at 25 mm downstream along the channel.

Q [mL h^{-1}]	Re [-]	c_L^- [-]	c_L^+ [-]	Channel length obtained by Equation 1 [mm]	Particles focusing regime at 25.0 mm downstream along the channel	
					Prediction	Experimental results
5.0	37	0.19	0.023	16.1	Tight focusing	Tight focusing
3.0	22	0.30	0.036	16.8	Tight focusing	Tight focusing
1.0	7.4	0.63	0.080	23.0	Tight focusing	Insufficient focusing
0.5	3.7	0.95	0.12	29.8	Insufficient focusing	Insufficient focusing
0.1	0.74	2.3	0.30	60.3	Insufficient focusing	Insufficient focusing

Table S2 Capture efficiencies and purities of the 13 and 7 μm beads achieved in the separation experiments using the CF-DLD.

Q [mL h^{-1}]	13 μm beads in outlet L			7 μm beads in outlet S		
	Capture efficiency [%]	Purity [%]	Number	Capture efficiency [%]	Purity [%]	Number
5.0	98.8	96.0	406	96.6	99.3	700
3.0	99.4	95.9	465	96.4	99.5	623
1.0	97.0	92.0	160	89.0	96.3	129
0.5	88.5	91.5	108	83.8	82.7	67

Table S3 Capture efficiencies and purities of the 13 and 7 μm beads at the different outlets in the separation experiments using the SF-DLD with different channel length of inertial focusing. The capture efficiencies and purities of the 7 μm beads were calculated based on the total number of beads collected at the two side outlets.

		13 μm beads at the center outlet (outlet L)			7 μm beads at the side outlets (outlet S_L and outlet S_R)		
Channel length [mm]	Q [mL h^{-1}]	Capture efficiency [%]	Purity [%]	Number	Capture efficiency [%]	Purity [%]	Number
2 mm	3.0	100	98.4	244	98.6	100	281
	1.0	97.1	95.6	66	97.3	98.2	107
5 mm	3.0	100	98.8	82	99.5	100	216
	1.0	98.4	98.4	62	98.5	98.5	67
20 mm	3.0	99.0	98.5	194	98.9	99.3	282
	1.0	98.0	99.0	100	99.2	98.4	123

Table S4 Numbers of the MCF-7 cells, WBCs, and RBCs collected at each outlet of the CF-DLD.

	After separation								
	Cell number at outlet L			Cell number at outlet S			Cell number at outlet V		
	MCF-7	WBCs	RBCs	MCF-7	WBCs	RBCs	MCF-7	WBCs	RBCs
#1/3	33	6	137	1	5	10875	0	0	480
#2/3	32	10	101	0	13	8561	0	2	637
#3/3	20	17	122	0	31	15066	0	9	650

<u>Supporting Movie Captions</u>

01_CF-DLD_up: Movie clip of the separation of MCF-7 cells from blood cells in the upstream CF-DLD, recorded at 2000 fps.

02_CF-DLD_mid: Movie clip of the separation of MCF-7 cells from blood cells in the midstream CF-DLD, recorded at 2000 fps.

03_CF-DLD_down: Movie clip of the separation of MCF-7 cells from blood cells in the downstream CF-DLD, recorded at 2000 fps.

All files are in MPEG-4 format.